Neuron, volume *61*

Supplemental Data

Millisecond-Timescale Optical Control of Neural Dynamics in the Nonhuman Primate Brain

Xue Han, Xiaofeng Qian, Jacob G. Bernstein, Hui-hui Zhou, Giovanni Talei Franzesi, Patrick Stern, Roderick T. Bronson, Ann M. Graybiel, Robert Desimone, and Edward S. Boyden

SUPPLEMENTAL RESULTS

Safety assessments. There are no defined immunostimulatory activities known to date to be associated with these light-activated channels. However, the membrane protein ChR2 (and the soluble protein GFP) are exogenously derived from non-primate organisms, raising the possibility that expression of such molecules in specific cells could, in theory, provoke an immune attack on those cells. Thus, we performed a series of different analyses to explore this possibility, focusing on brain regions with high densities of ChR2-GFP positive cells that were not immediately abutting the scar left by the cannula used for viral infusion. First, in the histological analysis of monkey N, performed 110 days after the first viral injection (and 81 days after the last viral injection), we saw ChR2-GFP expression in many excitatory cells (up to ~80%, near the center of injection sites). The widespread persistence of expression of these exogenous proteins in healthy-looking cells, several months after viral gene delivery**,** implies a lack of cytotoxic immune response against cells expressing ChR2-GFP (e.g., compare to (Aktas et al., 2005; Bien et al., 2002; Murphy et al., 2007)). Second, the recordings of neural activity modulated by light (**Figs. 3-4**) indicated functional expression of ChR2 in neurons throughout the period of the experiment (over 8 months for monkey A), even after many sessions of repeated blue-light illumination of the same set of cells. Third, to assess cellular architecture at the site of ChR2-GFP expression, we stained either the nuclei of all cells with the nucleic acid stain To-Pro-3 (**Fig. 2A**), or just the nuclei of neuronal cells with antibody to the neuron-specific nuclear marker NeuN (**Fig. 2B**). We did not detect disruptions of cellular architecture, even in regions with a high density of ChR2-GFP-expressing cells. Fourth, we measured the density of reactive astrocytes, using GFAP staining (Ridet et al., 1997). The density of GFAP-positive cells was identical in regions with a high density of ChR2-GFP expressing cells (13.5 ± 1.5 GFAP-positive cells per $2.5*10^6$ μm^3, mean ± SE) and in regions with no ChR2-GFP expressing cells, far away from the cannula (14.4 ± 1.5 GFAP positive cells per volume) ($p > 0.5$, unpaired t-test; n = 13 fields of view each), confirming that ChR2-GFP expression did not evoke gliosis. This lack of disorganization and immune cell infiltration was consistent with the excellent appearance of the ChR2-GFP-positive neurons (see also **Fig. 1**), as well as the physiological health of the neurons (**Fig. 3-4)**, even after many months of viral expression, and strongly suggests that a functional immune response did not occur.

Finally, we took a step towards assessing the presence of antibodies against ChR2-GFP in the serum of the two monkeys by Western blotting samples of their serum against purified membranes of HEK cells transfected with ChR2-GFP plasmids. Control western blotting with a rabbit polyclonal antibody against whole GFP consistently labeled two bands around 46 kD (approximately 75% of the molecular weight of the entire ChR2-GFP fusion protein, suggesting that we were consistently isolating two sizable fragments of the entire protein). These bands were detected only in the membrane fraction of HEK cells transfected with ChR2-GFP plasmid, and not in the cytosolic fraction of HEK cells transfected with ChR2-GFP plasmid, implying that we are indeed isolating a membrane-localized protein (**Fig. 2C**). These bands were not detected in membranes of untransfected HEK cells, confirming specificity of the antibody staining. Western blotting with monkey serum (1:50), obtained before vs. after viral injections, detected in neither case any specific reactivity to membranes of HEK cells transfected with ChR2-GFP, when compared to membranes of untransfected HEK cells (**Fig. 2D**). In greater detail: for both monkeys, there was nonspecific binding of serum to membranes of HEK cells, but there was no difference in binding of serum to membranes of ChR2-GFP transfected vs. untransfected HEK cells. Furthermore, there was no difference in the binding of serum to a given membrane extract, when we compared before vs. after virus injection. (The observed bands in the blotting of monkey serum against untransfected HEK cells do, however, suggest that our Western blot is capable of detecting some immune response in monkey serum, to a molecule found in untransfected cultured HEK cells.) Finally, we assessed the presence of antibodies in the monkey serum, by running the serum itself in a lane (**Fig. 2D**), and using a secondary antibody against monkey antibodies for visualization; this procedure revealed bands appropriate for antibodies in the serum (given that the heavy chain weighs ~50 kD). Taken together, these lines of evidence support a lack of productive immune response following neuron-specific expression of ChR2-GFP in primate brain.

Optical artifact at low frequencies on metal electrode tips in saline. When electrodes made of tungsten (as used in the in vivo recordings in monkey cortex reported in this paper) were immersed in saline, we observed a voltage deflection that occurred when the electrode tip was illuminated with light. Shown in **Supplemental Fig. 1A** are traces recorded on a tungsten electrode in saline being illuminated by a pulsed laser beam (120 mW). This voltage deflection was qualitatively proportional, in amplitude, to the magnitude of the incident light; the artifact was still visible when incident light power was reduced to 1% of the value that elicited the artifact in **Supplemental Fig. 1A**. The voltage slowly evolved over many tens of milliseconds, and accordingly was only recorded when the electrode voltage was measured on the low-frequency channel of the Plexon amplifier ("field potential channel," 0.7-170 Hz; **Supplemental Fig. 1Ai, ii,** *top traces*). This voltage deflection was not recorded when the electrode voltage was recorded on the high-frequency channel of the Plexon amplifier ("spike channel," 250-8000 Hz; **Supplemental Fig. 1Ai, ii,** *bottom traces*).

When light illuminated parts of the electrode other than the tip, no artifact was recorded; only illumination of the tip-saline interface resulted in the voltage transient. This phenomenon is consistent with a classical photoelectrochemical finding, the Becquerel

effect, in which illumination of an electrode placed in saline can produce a voltage on the electrode (Gratzel, 2001; Honda, 2004). Consistent with the generality of the Becquerel effect as a property of electrode-electrolyte interfaces, we observed this artifact even when the electrode material was switched to an alternative material, such as stainless steel, platinum-iridium, silver/silver chloride, gold, nichrome, or copper (data not shown). For a given positioning of electrode and light beam, and a given light power intensity, artifacts were observed to be stable in amplitude and timecourse, throughout the delivery of repeated light pulses. The artifact has been reported by another group using channelrhodopsin-2 as well, using silver electrodes for recording cortical responses (Ayling et al., 2009).

Similar slowly-evolving voltage deflections were observed when tungsten electrodes were used to record neural activity in the brain within a few millimeters of the fiber tip, during optical stimulation (**Supplemental Fig. 1Bi, ii,** *top traces*) with a radiant flux of 80 mW/mm^2 out the tip of the optical fiber (sufficient to activate neurons within about a cubic millimeter of brain, **Supplemental Figs. 2** and **5**). It is possible that part of this voltage deflection is due to the local field potential (LFP), but it is not possible in these data to resolve the LFP from the artifact. At a distance 1 millimeter away from the optical fiber tip, a distance at which optical neural activation was greatly reduced (**Supplemental Fig. 2**), the amplitude of the voltage deflection was reduced, but nonzero. Because the voltage deflection was slowly-evolving over many tens of milliseconds, spike waveforms were detected without corruption by the artifact, in the high-frequency channel of the Plexon amplifier (**Supplemental Fig. 1Bi, ii,** *bottom traces*). However, local field potentials and field oscillations, which reflect coherent neural dynamics in the range of Hz to tens of Hz, may be difficult to isolate from this Becquerel artifact using the electrodes here tested. We have not seen the artifact with pulled glass micropipettes (such as previously used in Boyden et al., 2005 and Han and Boyden, 2007, or in the mouse recordings described below). Thus, for recordings of local field potentials and other slow signals of importance for neuroscience, hollow glass electrodes may prove useful.

Dependence of light modulation of ChR2-expressing neurons upon light power and fiber position. We investigated the dependence of optical neural excitation on light amplitude by systematically decreasing the light intensity while recording from excited cells. We found, consistent with earlier reports in cultured neurons and in transgenic mice (e.g., (Boyden et al., 2005; Wang et al., 2007)), that light power intensity on the order of several mW/mm^2 were optimal for driving neural activity (n = 11; **Supplemental Fig. 2Ai-iii**). To explore the geometry of this situation for the primate brain, we recorded excited units, holding laser power intensity constant at 80 mW/mm^2, and retracted the optical fiber from its most efficacious position, in 200 micron increments. As expected, light-driven spiking decreased as the fiber was retracted (n = 7; **Supplemental Fig. 2Bi-iii**). Excited units lost their optical modulation fully when the optical fiber was retracted by an average of 1.2 ± 0.4 mm (mean ± SD), suggesting that a volume of about a cubic millimeter could be addressed in primate cortex, by a single fiber, at this power level. Interestingly, there was a noticeable trend for the after-light suppression of activity to vanish at lower light power intensities than did the beginning-of-light excitation of activity (e.g., compare the curves in **Supplemental Fig. 2Ai vs. Aiii**, or the curves in

Supplemental Fig. 2Bi vs. Biii). This observation is consistent with the idea that the suppression is mediated by distributed neural networks (presumably part of which is illuminated, even when the neuron being recorded is not being illuminated), whereas excitation requires immediate light delivery to the neuron being recorded (or perhaps to neurons very close by).

Excited and suppressed neural responses in mouse frontal cortex. To test whether the excited vs. suppressed responses observed (**Fig. 3**) were primate-specific, we repeated the experiment in rodent cortex. We injected FCK-ChR2-GFP lentivirus into the mouse frontal cortex (0.62 mm anterior, 0.5 mm lateral, and 0.5 mm deep, relative to bregma), so that ChR2-GFP was selectively expressed in excitatory neurons (37 of 37 GFP-positive neurons counted were α-CaMKII positive, whereas 0 of 32 GFP-positive neurons counted were GABA-positive). 4 weeks to 8 months after virus injection, we performed extracellular recordings on awake, head-fixed mice. 200 ms-duration blue light pulse illumination of ChR2-GFP-expressing excitatory neurons evoked both excited and suppressed responses in frontal cortical neurons (**Supplemental Fig. 3**). Thus, the heterogeneous responses observed in different neurons in the frontal cortex are not unique to the primate, but are also present in rodents, suggesting that simultaneous excited and suppressed responses may be a general property of cortical neural networks upon excitatory cell activation.

Spatial properties of viral labeling in primate frontal cortex. To assess the spatial extent of cells labeled by a single 1 μL virus injection in primate frontal cortex, we identified 6 well-isolated injection sites with clear borders and clear central cannula scars (such as the one shown in **Fig. 1D**). To estimate the diameter of the sphere containing ChR2-GFP expressing cells, we measured the fluorescence magnitudes along lines through the centers of virus injection sites (avoiding the cannula scar), as assessed in coronal slices (**Supplemental Fig. 4)**. Each injection of ~ 1 μl virus labeled a spherical region of ~1.4 mm in diameter (1.4 ± 0.5 mm, mean ± standard deviation (SD); n = 6 spheres of cells); the center cannula scar had an average diameter of 0.29 ± 0.07 mm (mean ± standard deviation; n = 6), similar to the actual diameter of the cannulas here used, of 0.25 mm.

Distribution of response types along individual electrode tracks. To probe the spatial distribution of excited and suppressed units, as well as of non-responsive units, we recorded neural responses in an unbiased fashion by advancing the electrode in 300 μm steps along a track, while keeping the fiber immobilized. The electrode position was, at each location, adjusted (± 40 microns) in the dark to optimize neural recording quality, and then illumination was performed to assess whether the recorded units fell into one of three response categories: excited, suppressed, or no response. Above or below certain depths along the track, presumably defined by the virus injection ball diameter (see above), chiefly unresponsive units were found. Between the farthest-separated depths along a track where units responded to light (e.g., either with excitation or suppression), practically all units recorded between these two depths were either excited or suppressed during light exposure (**Supplemental Fig. 5**), with only one non-responsive unit found in between responsive units during the five experiments shown. The distance between the

highest and lowest units recorded that were modulated by light ranged from 0.9-1.5 mm, consistent with the measurements of viral labeling (**Supplemental Fig. 4**) and the measurements of light delivery volume (**Supplemental Fig. 2**). Note that since units may have been multiunits, this experiment puts a lower bound on the fraction of non-responsive neurons in the observed regions (since if multiple neurons are recorded together and classified as one multiunit, then if any of the neurons are light-modulated, the entire multiunit will likely be classified as light-modulated). However, the fact that almost all cells recorded were modulated by light is consistent with the idea that the observed modulations were largely mediated by neural network-propagated activity, as the fraction of cells virally infected was significantly lower than 100%.

Rhythmic network activity mediated by ChR2 drive of excitatory cells in vivo. Rhythmic and oscillatory activity in the brain have been associated with many cognitive, emotional, sensory, and motor functions, raising the possibility that the ability to optically alter brain rhythms could lead to a better understanding of the causal role of such network dynamics in normal and pathological behavior. Accordingly, we probed the temporal precision of ChR2-driven network activity in primate cortex by exposing excited units to extended 10, 20, and 50 Hz trains of blue light pulses (pulse durations 20, 20, and 10 ms respectively) (**Supplemental Fig. 6**). Spike rates (measured during the 20 ms after the onset of each light pulse) elicited by each pulse declined somewhat during the course of each train, as evidenced by lower steady-state firing rates (mean response to the last 5 light pulses) than maximum firing rates (resulting from the first light pulse of the train) (10 Hz: $p < 0.005$, paired t-test, $n = 8$ units; 20 Hz: $p < 0.005$, $n = 14$ units; 50 Hz: $p < 0.05$, $n = 9$ units). In the steady state, light pulses resulted in spike rates that were 70%, 48% and 55% of those elicited by the first light pulses for 10 Hz, 20 Hz and 50 Hz trains, respectively (**Supplemental Fig. 6Aii, Bii, Cii**). Thus, while spiking could still be reliably elicited by pulse train protocols over an extended time, the probability of firing decreased somewhat throughout such trains, especially at pulse rates 20 Hz and higher. Even so, the trial-to-trial jitter of the spikes was ~4 ms, averaged across units (**Supplemental Fig. 6Aiii, Biii, Ciii)**, and did not change throughout the trains ($p > 0.1$ for all frequencies, paired t-test). Thus, spike timing remained reliable across a wide range of frequencies, despite a reduction in firing probability throughout long, high-frequency pulse trains, suggesting that ChR2-mediated drive of excitatory cells may enable the probing of the role of neural synchrony in cortical computation.

SUPPLEMENTAL FIGURE LEGENDS

Supplemental Figure 1. Voltage deflections observed on tungsten electrodes immersed in saline (**A**) or brain (**B**), upon tip exposure to 200 ms blue light pulses (**i**) or trains of 10 ms blue light pulses delivered at 50 Hz (**ii**). Light pulses are indicated by blue dashes. Electrode data was hardware filtered using two data acquisition channels operating in parallel, yielding a low-frequency component ("field potential channel") and a high-frequency component ("spike channel"). For the "spike channel" traces taken in brain (**B**), spikes were grouped into 100 ms bins, and then the binned spikes were displayed beneath corresponding parts of the simultaneously acquired "field potential channel"

signal (59 and 53 repeated light exposures for **Bi** and **Bii** respectively). (Shown are the spikes in 8 such bins – the 2 bins before light onset, the 2 bins during the light delivery period, and the 4 bins after light cessation.) For all other signals shown, 10 overlaid traces are plotted.

Supplemental Figure 2. Light intensity dependence of neural activity driven by ChR2-mediated activation of excitatory neurons. **A**, neural activity during 'Beginning of light' (**i**), 'Steady state' (**ii**), and 'After light' (**iii**) time periods, upon illumination with different light power intensities (plotted is mean ± SE; n = 11 excited units). **B**, neural activity during 'Beginning of light' (**i**), 'Steady state' (**ii**), and 'After light' (**iii**) periods, when optical fibers were retracted, holding the electrode still (plotted is mean ± SE; n = 7 excited units).

Supplemental Figure 3. Increases and decreases in firing rates of neurons in mouse frontal cortex, during optical stimulation of excitatory neurons. **A**, increases in spiking activity in one neuron during blue light illumination (200 ms duration). *Top,* spike raster plot displaying each spike as a black dot; 25 trials are shown in horizontal rows, in this and subsequent raster plots; *bottom*, histogram of instantaneous firing rate (averaged across all trials; bin size, 5 ms, in this and subsequent histogram plots). **B**, decreases in spiking activity in one neuron during blue light illumination (200 ms duration). *Top,* spike raster plot; *bottom*, histogram of instantaneous firing rate.

Supplemental Figure 4. Fluorescence magnitudes measured along lines taken through the centers of spheres of virally-labeled neurons, each created by one injection of 1 microliter of ChR2-GFP lentivirus. Shown are the mean (black lines) and the mean $\pm$ SD (gray lines) for n = 6 well-isolated spheres of virally-labeled cells.

Supplemental Figure 5. Quantitation of the number of light-responsive and light-unresponsive units detected along five individual electrode tracks, each sampled every 300 microns. The farthest-separated depths where units responded to light were first identified, and each unit recorded between those two depths was then classified according to its activity profile – excitation, suppression, or nonresponsive – during light illumination.

Supplemental Figure 6. Driving oscillatory cortical activity by activating ChR2 expressing excitatory neurons with rhythmic blue light pulse trains, at 10 Hz (**A**), 20 Hz (**B**), and 50 Hz (**C**). For each of these three pulse rates, plotted in subpanel **i** is the histogram of instantaneous firing rate (bin size, 5 ms) averaged across all excited units tested (black lines, mean; gray lines, mean ± SE; n = 8 units for 10 Hz, n = 14 units for 20 Hz, and n = 9 units for 50 Hz). Plotted in subpanel **ii** is the firing rate divided by baseline firing rate, during the 20 ms following the onset of each light pulse, and averaged across all excited units tested (mean ± SE)). Plotted in subpanel **iii** is the jitter of spike times elicited by each pulse, calculated as the across-trial standard deviation of the time of the first spike elicited within 20 ms of each light pulse onset and averaged across all excited units tested (mean ± SE).

SUPPLEMENTAL EXPERIMENTAL PROCEDURES

Virus design and production. Replication-incompetent VSVg-pseudotyped lentivirus was produced via triple transfection of FCK-ChR2-GFP lentiviral plasmid (available at http://www.addgene.org/pgvec1?f=c&cmd=findpl&identifier=15814), the viral helper plasmid (pΔ8.74, information at http://www.addgene.org/pgvec1?vectorid=5682&f=v&cmd=showvecinfo), and the pseudotyping plasmid pMD2.G, encoding for the VSVg coat protein (http://www.addgene.org/pgvec1?f=c&cmd=findpl&identifier=12259). VSVg was used because it enables viral infection of a wide range of cell types, including neurons *in vivo* (Naldini et al., 1996). HEK293FT cells (Invitrogen) were plated onto four T175 flasks in D10 medium (DMEM + 10% FBS + 1% penicillin-streptomycin + 1% sodium pyruvate). At near 100% confluence, cells were transfected with DNA (per flask: 22 μg FCK-ChR2-GFP, 15 μg pΔ8.74, 7 μg pMD2.G, 132 μL Fugene 6, brought up to 4.5 mL with DMEM, mixed according to the Fugene instructions, and then added to 16 mL of D10). 24 hours later, the cells were given 20 mL of virus production media (Ultraculture (Lonza) + 1% penicillin-streptomycin + 1% sodium pyruvate +1% sodium butyrate). 48 hours later, the supernatant was spun down at 2000 rpm in a Beckman benchtop Allegra centrifuge for 5 min, filtered through a 0.45 micron filter, and then ultracentrifuged at 22000 rpm in a SW-28 rotor, through a 20% sucrose + phosphate buffered saline (PBS) cushion, for 2 hours at 4°C. The pellets were then slowly resuspended in 30-100 microliters of PBS, and aliquotted in single-use aliquots for storage at −80°C. This protocol enabled production of clean, non-toxic, high-titer (roughly estimated at ~10^9 infectious units/mL) lentivirus for injection into the brain.

General surgical procedures. Two rhesus monkeys (*Macaca mulatta*), 7-11 years of age, weighing 8-15 kg, were used. All procedures were in accordance with the National Institutes of Health Guide for the care and use of Laboratory Animals and approved by the Massachusetts Institute of Technology Animal Care and Use Committee. Under isoflurane anesthesia, a titanium headpost and recording chambers were surgically affixed to the skull, and a craniotomy opened up in one or more of the chambers, according to MRI-determined coordinates for the periarcuate regions (premotor/FEF areas) of the frontal cortex.

Virus injection. The virus was injected through a 31-gauge stainless steel cannula held in a microdrive (Plexon NAN Drive) attached to the recording chamber while the monkey was seated in a primate chair. The cannula was connected via polyethylene tubing to a Hamilton syringe, placed in a syringe pump (Harvard Apparatus), and the syringe, tubing, and cannula filled with silicone oil (Sigma). To insure the ability to both target virus to the desired area, and to return to the same site later for reliable electrophysiology and optical control, we designed a custom 3-D targeting grid using Solidworks (Solidworks Corp.), and printed it out of acrylic (VisiJet SR 200 Plastic Material acrylic) with a 3-D printer with ~50-micron resolution (3D Systems, Inc.). This grid is analogous to commercially available grids from Crist Instrument Co., but tuned for the specific geometries of interest for this joint electrical-optical experiment. One microliter of virus

was injected over a 10 minute period. We then waited an extra 10 minutes for the virus to diffuse away from the site of injection before withdrawing the cannula at a slow rate of 0.12-0.3 mm/min.

The injection strategy was designed to target cortical tissue on each side (posterior and anterior) of the arcuate sulcus (i.e., premotor cortex and FEF, respectively). Thus, to hit the deepest targets of the sulcus, a deeper termination point was required (i.e., we stopped the injector 7 mm below the dura) than to hit targets more anterior or more posterior to the sulcus (i.e., we stopped the injector 5 mm below the dura). The angle of the injection was approximately vertical, and ultimately governed by the placement of the chamber on the skull. Viral injection was accomplished by lowering a 31-gauge steel cannula (250 microns in diameter) into a given site in the grid, targeting the depth as described above, and then injecting 1 μL of FCK-ChR2-GFP virus at that depth. Then, we repeatedly (4-6 times, as appropriate) retracted the injector in 1 mm steps, injecting an additional 1 μL each time, until the cannula was fully retracted. In this way, we attempted to label large regions on both sides of the arcuate sulcus.

Optical stimulation hardware. A 200 mW blue laser (A-L473-200, Aixiz) was coupled to a 200 micron-diameter optical fiber (FIBER-200-UV, Ocean Optics, although sometimes we also used 100 micron fibers) through a homebuilt collimator setup (AC254-040-A1-ML lens, mounted on a modified SM1L20 lens tube, and attached to a SM1SMA fiber adapter, the assembly of which was mounted on a KM100T mirror mount, all from Thorlabs). To prepare the fiber to connect to our homebuilt collimator assembly, we used an SMA connector terminator kit (TERM-KIT, Ocean Optics). The laser, collimator, and mirrors (BB1-E02, mounted on KM100 mirror mounts, Thorlabs), were mounted on a standard optics breadboard (MB1824, Thorlabs), as outlined in (Bernstein et al., 2008). Laser light power was measured with an 818-SL photodetector (Newport Co.)

The fiber was then placed into a stainless steel cannula slightly larger than the optical fiber, and then guided into the brain, using the same electrode drive described above. The laser was controlled via TTL pulses driven by a pulse generator (DS8000, WPI Inc.), with the timing controlled by a computer through the software package, Cortex (http://www.cortex.salk.edu/).

Electrophysiological recording and optical stimulation. Standard tungsten electrodes of 1-2 MΩ resistance (FHC, Inc.) were guided into the brain along a track parallel to the fiber (separated by 0-600 μm), via a second drive. The guide tubes holding the electrode and holding the fiber were often glued parallel to one another, so that fibers and electrodes would remain laterally spaced within 0.6 mm of one another throughout the experiment (recording more lateral to the fiber reduced the probability of obtaining optically modulated cells, although we did not quantitate this in detail). Fibers and electrodes were lowered separately through their respective guide tubes at a slow rate of ~1.5 μm/s to minimize any potential deformation of the cortical surface. Guide tubes did not enter the brain, but instead rested outside the dura; only the fibers and electrodes entered, lowered through the guide tubes.

Data amplification, filtering and acquisition were performed with a Multichannel Acquisition Processor (MAP) system (Plexon, Inc.), which contains multiple data acquisition channels. Each data acquisition channel is split into two parallel channels and filtered with two different bandpass filters to reveal content at different frequencies. The "spike channel" used throughout this paper is defined by Plexon as 250 Hz – 8 kHz and sampled at 40 kHz. The other channel, the "field potential channel," is defined by Plexon as 0.7 Hz -170 Hz. Spikes recorded on the spike channel were semi-automatically detected using an interactively-set threshold, and the spike waveforms were offline sorted to distinguish putative single vs. putative multiple units using principal component analysis (PCA) (Offline Sorter, Plexon, Inc.). Most of the neurons recorded had broad spike waveforms with trough-to-peak duration >250 μs (3 out of 31 single neurons had trough-to-peak waveform durations of 100-200 μs, and the rest had trough-to-peak waveform durations of 250-425 μs), indicating that most of the recorded neurons were putative excitatory neurons (Mitchell et al., 2007). Spike timing was defined as the moment of threshold crossing. Light resulted in a slow artifact on the electrode (**Supplemental Fig. 1**), which was easily separable from the spike trains through high-pass filtering.

During the experiment, one fiber and one or more electrodes were lowered into the brain of an awake headfixed monkey, and optical stimulation was performed while units were recorded. During the recording period, the monkeys were awake and freely viewing, in a dimly lit room. Our targets in arcuate sulcus contain premotor areas; we did not observe overt eye or limb movements during experiments with the stimuli used. Occasional juice rewards were delivered to insure alertness, but no tasks nor reward contingencies were scheduled in the described recording sessions. Our recording strategy was to position the electrode near the fiber by searching for the slow light-induced artifact, and then optimizing the electrode position to record neurons. Subregions of the targeted areas could be found in which no units were modulated by light, and subregions were also found in which almost 100% of the units were modulated by light (**Supplemental Fig. 5**).

Artifact characterization in saline. Electrodes were positioned in saline and targeted by the laser beam. Voltage deflections were amplified, filtered and acquired with a Multichannel Acquisition Processor (MAP) system (Plexon, Inc.). Specifically, the "field potential channel" is defined by Plexon as 0.7-170 Hz and sampled at 1 kHz or 20 kHz. The "spike channel" is defined by Plexon as 250 Hz – 8 kHz and sampled at 20 kHz or 40 kHz.

Electrophysiology data analysis. Electrophysiological data analysis was performed using MATLAB (Mathworks, Inc.). Light-modulated neurons were identified and classified by performing a paired t-test, for each neuron, between the firing rate during the 200 ms period before light onset ('baseline firing rate') vs. during the period of light exposure, across all trials for that neuron, and thresholded at the $p < 0.05$ significance level. Units that showed significant increases in firing rate during any of three time periods – the first 20 ms of light exposure ('Beginning of light'), the period between 20 ms after light onset and 20ms after light cessation ('Steady state'), and during the 20 ms

period starting 20 ms after light cessation ('After light') – were defined as excited units. Units that showed no increase in firing rate during any of these three periods, but showed reduction in firing rate during any of the periods, were defined as suppressed units. To determine the latency between light onset and the neural response (or, for **Fig. 3M**, the time for after-light suppression to recover back to baseline), we swept a 6 ms-long sliding window through the electrophysiology data and looked for the earliest 6 ms period that deviated from baseline firing rate, as assessed by performing a paired t-test for the firing rate during each window vs. during the baseline period, across all trials for each neuron. Latency was defined as the time from light onset to the time at which firing rate was significantly different from baseline for the following 12 ms. Normalizing firing rate at a given timepoint to baseline was performed by taking the ratio of firing rate at that timepoint, to the baseline firing rate. Firing rate change during a given period was defined as the firing rate during that period, minus the baseline firing rate. Jitter was defined as the standard deviation, across repeated trials, of the timing of the first spike that occurred after the onset of a light pulse.

Mouse optical activation and recording. Adult Swiss Webster or C57 mice were used. All procedures were in accordance with the National Institutes of Health Guide for the care and use of Laboratory Animals and approved by the Massachusetts Institute of Technology Animal Care and Use Committee. Under isoflurane anesthesia, 1 μL lentivirus made with FCK-ChR2-GFP was injected through a craniotomy to the premotor area (0.62 mm anterior, 0.5 mm lateral, and 0.5 mm deep, relative to bregma). A custom-fabricated plastic headpost was affixed to the skull, and the craniotomy was protected with agar and covered with a plastic plate. Recordings (cell-attached or extracellular recordings) were made on headfixed, awake mice up to 8 months after virus injection, using glass microelectrodes of ~5MΩ filled with PBS, containing silver/silver-chloride wire electrodes. Signals were amplified with a Multiclamp 700B amplifier, digitized with a Digidata 1440 and acquired with pClamp 10 (Molecular Devices). Data analysis was with Matlab.

Histology and immunofluorescence. One of the two monkeys, Monkey N, weight 8.6 kg, was deeply anesthetized with an overdose of pentobarbital (>70 mg/kg, i.v.), and then the borders of the 3-D targeting grid were marked in the brain by insertion of 18-gauge cannulas into grid holes near the corners. Then the animal was immediately perfused through the left ventricle, first with phosphate buffered saline (PBS; pH 7.3) (2 liters), then with 4% paraformaldehyde in PBS (4 liters), followed by 2 liters of PBS. The cannulas were then removed, and the brain was blocked and cryoprotected in PBS with 20% glycerol + 0.1% sodium azide (>2 days). Brains were then cut into 60 μm coronal sections on a sliding microtome, and stored in PBS + 0.1% sodium azide.

Brain slices were washed and permeabilized 3 times for 30 minutes each in a solution containing PBS, 100 mM glycine, and 0.5% triton X-100 (PTG solution), and then blocked for 2 hours in PTG + 2% normal goat serum from Jackson Immunochemicals (PTB solution). Slices were then incubated with primary antibody in PTB solution overnight at 4^{o}C on a shaker, then washed 4 times for 30 minutes each with PTG solution, and then incubated in the secondary antibody in PTB solution for 2 hours at

room temperature. Finally, the slices were washed 3 times for 30 minutes each with PTG solution, and for 30 minutes in PBS + 100 mM glycine. Antibodies and stains used were rabbit anti-α-CaMKII (1:50, Santa Cruz Biotechnology), rabbit anti-GABA (1:500, Sigma), rabbit anti-GFAP (1:1000, Upstate), mouse anti-NeuN (1:1000, Chemicon), To-Pro–3 iodide (1:2000, Invitrogen), chicken anti-GFP (1:500, Chemicon), Alexa 488 goat anti-chicken (1:500), and Alexa 568 goat anti-rabbit (1:500) (Invitrogen). Slices were mounted with Vectashield solution (Vector Labs), and visualized with a Zeiss LSM Pascal confocal microscope.

Confocal data analysis of immunostaining and cell counting was performed by taking 3-D z-stacks with a 63x oil lens (Zeiss), each 202 x 202 x 60 microns in volume. To maximize accuracy of overlap determination and cell counting, cells were first identified on the green (ChR2-GFP) and red (cell-type marker) channels separately, then overlap was assessed.

For measuring the diameters of the spheres of virally-labeled cells, images containing well-isolated spheres of GFP fluorescence (n = 6 such sites) were taken using an Olympus fluorescence microscope (using 4x or 10x objective lenses). We measured the diameter of each virus sphere as follows, using ImageJ (NIH): first, we visually estimated the center of each virus sphere by examining each section through the virus sphere, and drew a randomly-oriented line through this center. (In choosing this line we did, however, avoid the cannula injection hole.) Then, we extracted the magnitudes of the fluorescence values for each pixel along this line, after performing a flat-field correction. The diameter of the spheres of GFP fluorescence was then determined as the distance between the two points at which the fluorescence fell to 20% of the peak, defined as the median of the 50 highest fluorescence values along the line. To facilitate comparison of different images for statistical purposes, we normalized each set of magnitudes to the peak, and identified the midpoint as halfway between the two points at which the fluorescence fell to 20% of the peak. For the population data (**Supplemental Fig. 4**), the normalized curves were aligned at their midpoints, and mean and standard deviation were calculated.

Western blotting. Non-human primate blood samples were collected in a Sarstedt Serum Monovette tube, and centrifuged in a Hettich Rotofix 32 Centrifuge at 2,000 RPM for 10 minutes. The serum was then transferred into a Sarstedt screw cap storage tube and then stored at -80 °C until ready for analysis. HEK cell membranes containing ChR2-GFP were prepared by transfecting 10-cm plates of HEK cells with ChR2-GFP under the CAG promoter. 3 days later, the cells from one such plate, as well as one control plate, were resuspended in PBS and centrifuged for 10 min at 2000 rpm in a benchtop centrifuge at 4^{o}C. Cell pellets were resuspended in 1 ml PBS with proteinase inhibitors (Roche), lysed in a cup sonicator for 15 seconds and centrifuged for 2 minutes at 13,000 rpm at 4^{o}C. The pelleted membranes were then resuspended in 0.5 ml Laemmli sample buffer containing SDS (Bio-Rad Inc.). For Western blotting, wells of 12% polyacrylamide gels (Bio-Rad Inc.) were loaded with 15 μl of this solution, or of a 1:5 dilution thereof. Additionally, some wells were loaded with 0.02 μL of monkey serum (a total of 15 μL, containing 1:750 diluted monkey serum), in order to assay the antibody content. After electrophoresis, proteins were transferred from the gel to a PVDF membrane (Bio-Rad

Inc.), which was then washed for 10 mins in TBS (20 mM Tris/HCl and 150 mM NaCl, pH, 7.4), blocked with 3% BSA in TBS for 2 hours, then washed and incubated with rabbit-anti-GFP antibody (1:1000, Invitrogen) or monkey serum for 2 hours at 4^{o}C while shaking. The PVDF membrane was then washed 3 times for 10 mins each, with 0.5% Tween 20 in TBS, followed with washing in TBS once, and then incubated with horseradish peroxidase (HRP)-conjugated goat-anti-rabbit or rabbit-anti-monkey secondary antibody (1:80,000, Sigma) for 2 hours. The PVDF membrane was then washed again, as described above. HRP was then imaged by adding Western Lightning Chemiluminescence Reagent Plus substrate (PerkinElmer).

REFERENCES

Aktas, O., Smorodchenko, A., Brocke, S., Infante-Duarte, C., Schulze Topphoff, U., Vogt, J., Prozorovski, T., Meier, S., Osmanova, V., Pohl, E.*, et al.* (2005). Neuronal damage in autoimmune neuroinflammation mediated by the death ligand TRAIL. Neuron *46*, 421-432.

Ayling, O.G., Harrison, T.C., Boyd, J.D., Goroshkov, A., and Murphy, T.H. (2009). Automated light-based mapping of motor cortex by photoactivation of channelrhodopsin-2 transgenic mice. Nat Methods.

Bernstein, J.G., Han, X., Henninger, M.A., Ko, E.Y., Qian, X., Franzesi, G.T., McConnell, J.P., Stern, P., Desimone, R., and Boyden, E.S. (2008). Prosthetic systems for therapeutic optical activation and silencing of genetically-targeted neurons. Proceedings - Society of Photo-Optical Instrumentation Engineers *6854*, 68540H.

Bien, C.G., Bauer, J., Deckwerth, T.L., Wiendl, H., Deckert, M., Wiestler, O.D., Schramm, J., Elger, C.E., and Lassmann, H. (2002). Destruction of neurons by cytotoxic T cells: a new pathogenic mechanism in Rasmussen's encephalitis. Ann Neurol *51*, 311-318.

Boyden, E.S., Zhang, F., Bamberg, E., Nagel, G., and Deisseroth, K. (2005). Millisecond-timescale, genetically targeted optical control of neural activity. Nat Neurosci *8*, 1263-1268.

Gratzel, M. (2001). Photoelectrochemical cells. Nature *414*, 338-344.

Honda, K. (2004). Dawn of the evolution of photoelectrochemistry. Journal of Photochemistry and Photobiology A: Chemistry *166*, 63-68.

Mitchell, J.F., Sundberg, K.A., and Reynolds, J.H. (2007). Differential attention-dependent response modulation across cell classes in macaque visual area V4. Neuron *55*, 131-141.

Murphy, K.M., Travers, P., and Walport, M. (2007). Janeway's Immunobiology, 7th edn.

Naldini, L., Blomer, U., Gallay, P., Ory, D., Mulligan, R., Gage, F.H., Verma, I.M., and Trono, D. (1996). In vivo gene delivery and stable transduction of nondividing cells by a lentiviral vector. Science *272*, 263-267.

Ridet, J.L., Malhotra, S.K., Privat, A., and Gage, F.H. (1997). Reactive astrocytes: cellular and molecular cues to biological function. Trends Neurosci *20*, 570-577.

Wang, H., Peca, J., Matsuzaki, M., Matsuzaki, K., Noguchi, J., Qiu, L., Wang, D., Zhang, F., Boyden, E., Deisseroth, K.*, et al.* (2007). High-speed mapping of synaptic connectivity using photostimulation in Channelrhodopsin-2 transgenic mice. Proc Natl Acad Sci U S A *104*, 8143-8148.

Han et al., Supplementary Figure 1

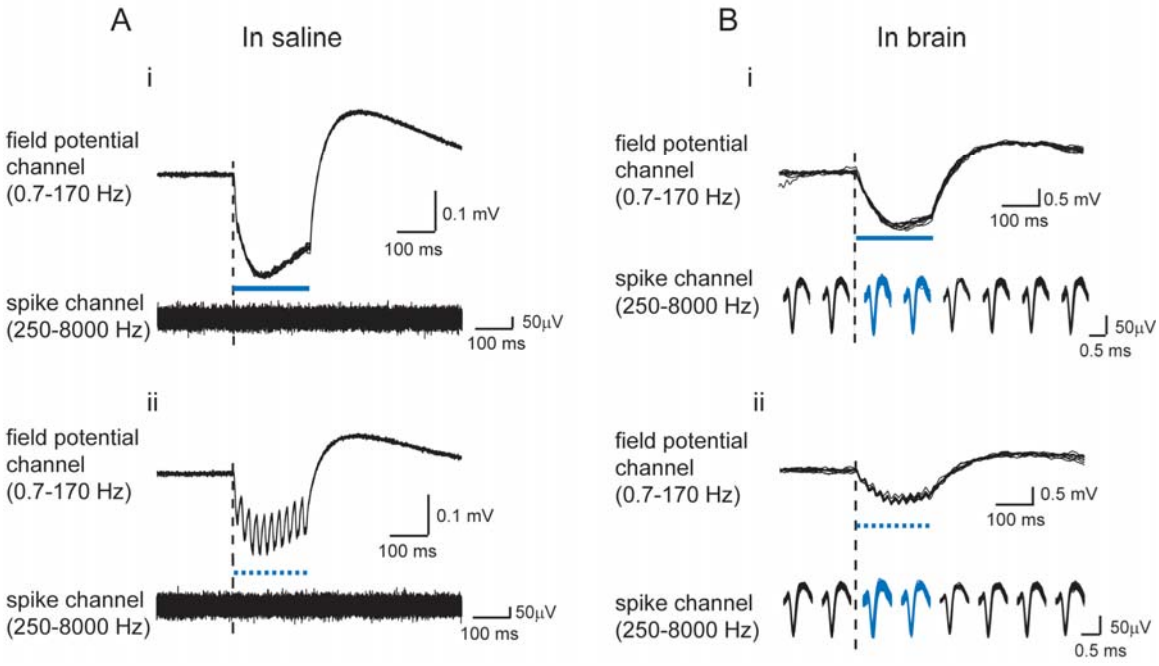

Han et al., Supplementary Figure 2

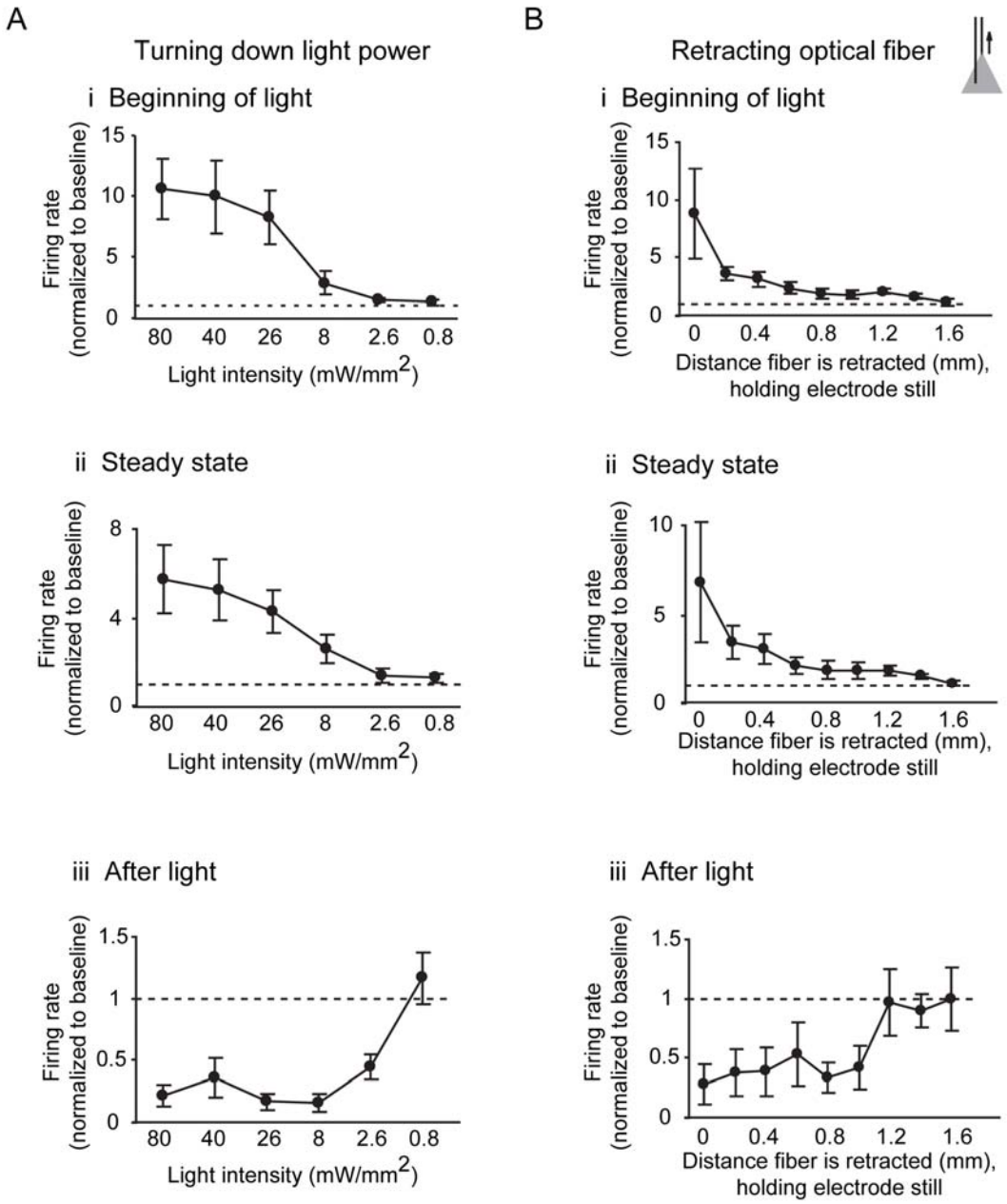

Han et al., Supplementary Figure 3

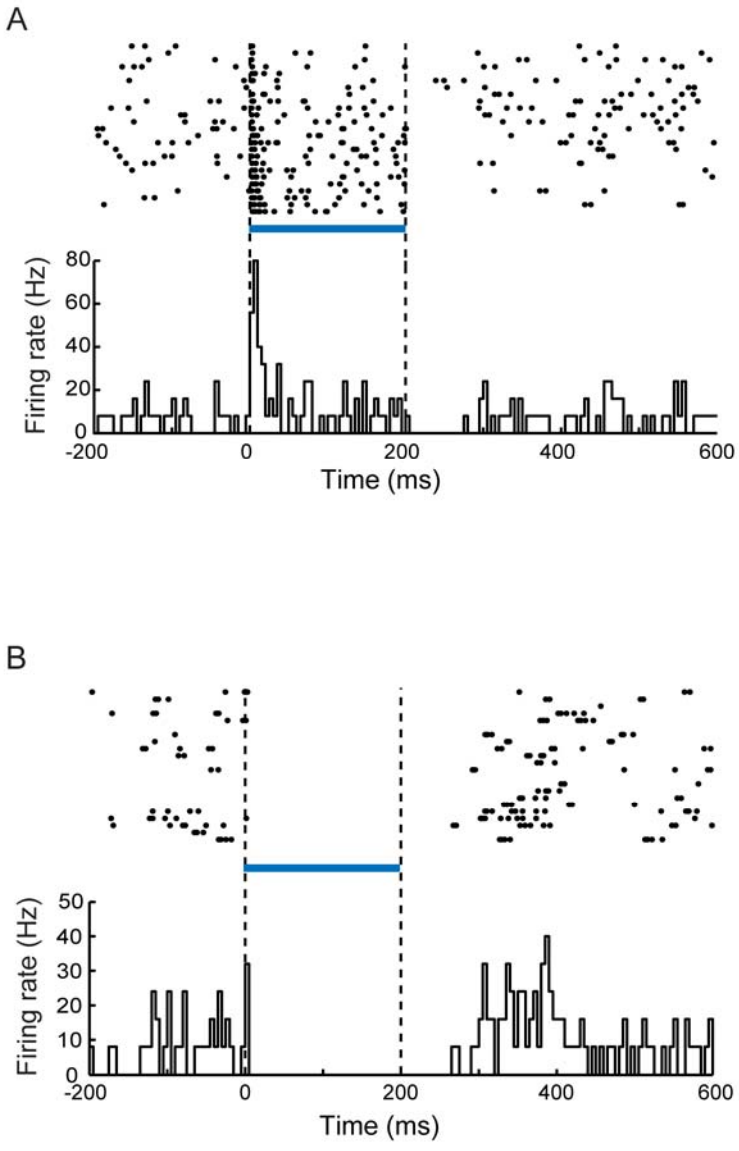

Han et al., Supplementary Figure 4

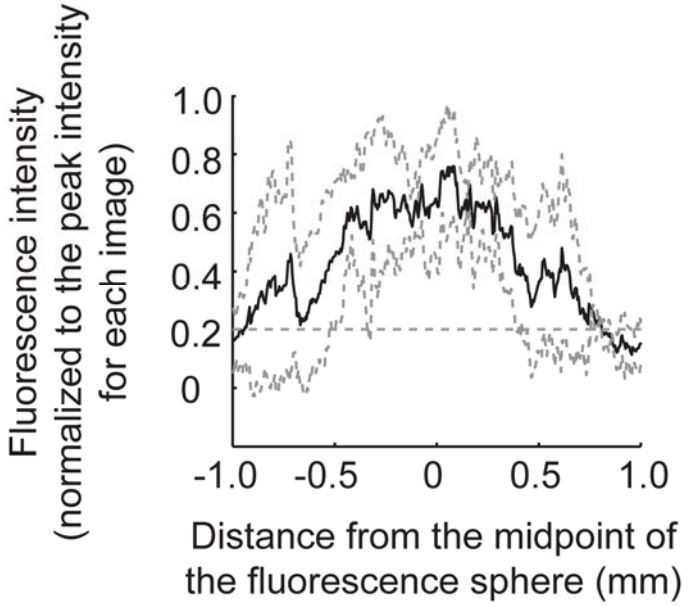

Han et al., Supplementary Figure 5

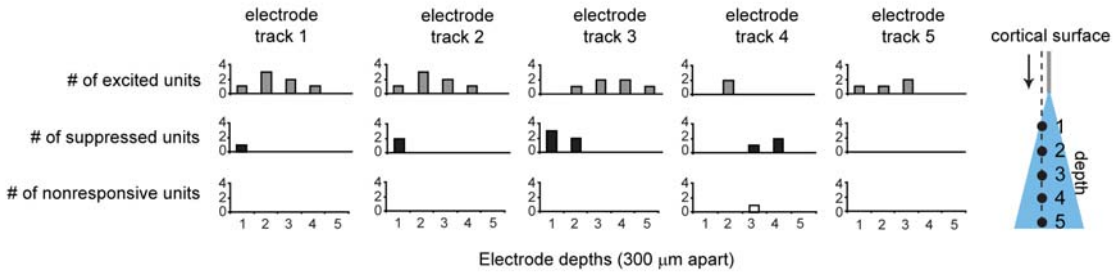

Han et al., Supplementary Figure 6